

Testing Higgs models via the $H^\pm W^\mp Z$ vertex by a recoil method at the International Linear Collider

Shinya Kanemura,^{1,*} Kei Yagyu,^{1,†} and Kazuya Yanase^{1,‡}

¹*Department of Physics, University of Toyama,
3190 Gofuku, Toyama 930-8555, Japan*

Abstract

In general, charged Higgs bosons H^\pm appear in non-minimal Higgs models. The $H^\pm W^\mp Z$ vertex is known to be related to the violation of the global symmetry (custodial symmetry) in the Higgs sector. Its magnitude strongly depends on the structure of the exotic Higgs models which contain higher isospin $SU(2)_L$ representations such as triplet Higgs bosons. We study the possibility of measuring the $H^\pm W^\mp Z$ vertex via single charged Higgs boson production associated with the W^\pm boson at the International Linear Collider (ILC) by using the recoil method. The feasibility of the signal $e^+e^- \rightarrow H^\pm W^\mp \rightarrow \ell\nu jj$ is analyzed assuming the polarized electron and positron beams and the expected detector performance for the resolution of the two-jet system at the ILC. The background events can be reduced to a considerable extent by imposing the kinematic cuts even if we take into account the initial state radiation. For a relatively light charged Higgs boson whose mass m_{H^\pm} is in the region of $120\text{--}130 \text{ GeV} < m_{H^\pm} < m_W + m_Z$, the $H^\pm W^\mp Z$ vertex would be precisely testable especially when the decay of H^\pm is lepton specific. The exoticness of the extended Higgs sector can be explored by using combined information for this vertex and the rho parameter.

PACS numbers: 12.60.Fr, 14.80.Fd

Keywords: Extended Higgs sector, Charged Higgs boson, Collider Physics

*Electronic address: kanemu@sci.u-toyama.ac.jp

†Electronic address: keiyagyu@jodo.sci.u-toyama.ac.jp

‡Electronic address: yanase@jodo.sci.u-toyama.ac.jp

I. INTRODUCTION

Physics of electroweak symmetry breaking remains unknown, and its exploration is crucial to establish our standard picture for the origin of masses of elementary particles. The structure of the Higgs sector may not necessarily be the minimal form in the standard model (SM). Extended Higgs sectors have often been considered in various new physics contexts beyond the SM. Therefore, determination of the Higgs sector is also important to obtain clue to a new paradigm for physics at the TeV scale. The Higgs boson search is currently one of the most important tasks at the Fermilab Tevatron and the CERN Large Hadron Collider (LHC).

Basic properties in an extended Higgs sector are the number of the scalar fields as well as their representation under the isospin $SU(2)_L$ and the hypercharge $U(1)_Y$. An important observable to constrain the structure of extended Higgs models is the electroweak rho parameter ρ , whose experimental value is very close to unity; $\rho_{\text{exp}} = 1.0008^{+0.0017}_{-0.0007}$ [1]. This fact suggests that a global $SU(2)$ symmetry (custodial symmetry) plays an important role in the Higgs sector. In the Higgs model which contains complex scalar fields with the isospin T_i and the hypercharge Y_i as well as real ($Y = 0$) scalar fields with the isospin T'_i , the rho parameter is given at the tree level by

$$\rho_{\text{tree}} = \frac{\sum_i [|v_i|^2(T_i(T_i + 1) - Y_i^2) + u_i^2 T'_i(T'_i + 1)]}{2 \sum_i |v_i|^2 Y_i^2}, \quad (1)$$

where v_i (u_i) represents the vacuum expectation value (VEV) of the complex (real) scalar field [2]. In the model with only scalar doublet fields (and singlets), we obtain $\rho_{\text{tree}} = 1$ so that the natural extension of the Higgs sector is attained by adding extra doublet fields and singlet fields [3]. In these models, radiative corrections can provide a deviation from unity. It is well known that in the SM with one Higgs doublet field, the mass $m_{H_{SM}}$ of the Higgs boson H_{SM} is strongly constrained from above through the quantum effect on the rho parameter ($m_{H_{SM}} < 144$ GeV at 95% C.L.) [4]. This bound is clearly model dependent in the non-minimal Higgs sector. On the other hand, addition of the Higgs field with the isospin larger than one half can shift the rho parameter from unity at the tree level, whose deviation is proportional to the VEVs of these exotic scalar fields. The rho parameter, therefore, has been used to exclude or to constrain a class of Higgs models [5].

A common feature in the extended Higgs models is the appearance of physical charged scalar components. Most of the extended Higgs models contain singly charged Higgs bosons

H^\pm . Hence, we may be able to discriminate each Higgs model through the physics of charged Higgs bosons. In particular, the $H^\pm W^\mp Z$ vertex can be a useful probe of the extended Higgs sector [6–9]. Assuming that there are several physical charged scalar states H_α^\pm ($\alpha \geq 2$) and the Nambu-Goldstone modes H_1^\pm , The vertex parameter ξ_α in $\mathcal{L} = igm_W \xi_\alpha H_\alpha^+ W^- Z + \text{h.c.}$ is calculated at the tree level as [6]

$$\sum_{\alpha \geq 2} |\xi_\alpha|^2 = \frac{1}{\cos^2 \theta_W} \left[\frac{2g^2}{m_W^2} \left\{ \sum_i [T_i(T_i + 1) - Y_i^2] |v_i|^2 Y_i^2 \right\} - \frac{1}{\rho_{\text{tree}}^2} \right], \quad (2)$$

where ρ_{tree} is given in Eq. (1). A non-zero value of ξ_α appears at the tree level only when H_α^\pm comes from an exotic representation such as triplets. Similarly to the case of the rho parameter, the vertex is related to the custodial symmetry. In general, this can be independent of the rho parameter. If a charged Higgs boson H_α^\pm is from a doublet field, ξ_α vanishes at the tree level. The vertex is then one-loop induced and its magnitude is proportional to the violation of the global symmetry in the sector of particles in the loop. Therefore, the determination of the $H^\pm W^\mp Z$ vertex can be a complementary tool to the rho parameter in testing the *exoticness* of the Higgs sector.

It goes without saying that the decay of H^\pm is strongly model dependent. If H^\pm comes from multi-doublet models it can couple to quarks and leptons via Yukawa interaction which is classified in terms of the softly-broken discrete Z_2 symmetry to avoid the flavor changing neutral current [10–12]. On the other hand, if H^\pm is originated from higher representation fields such as triplets, the coupling to quarks is forbidden because of the $U(1)_Y$ hypercharge invariance. Therefore, the decay of charged Higgs bosons from exotic Higgs sectors is mainly leptophilic, and they can only couple to quarks through mixing with doublet-like charged scalars.

There have been lots of studies on collider phenomenology for charged Higgs bosons. At hadron colliders such as the Tevatron and the LHC, a main production mechanism may be the one from top-quark decay from top-quark pair production if $m_{H^\pm} < m_t + m_b$ [16]. Otherwise, H^\pm may be produced via $gg(q\bar{q}) \rightarrow tbH^\pm$ [17], $gg(b\bar{b}) \rightarrow W^\pm H^\mp$ [18], $gg(q\bar{q}) \rightarrow H^+ H^-$ [19, 20], $q\bar{q}' \rightarrow W^* \rightarrow \phi^0 H^\pm$ [21], $q\bar{q}' \rightarrow W^* \rightarrow H^\pm H^{\mp\mp}$ [22], $q\bar{q} \rightarrow q\bar{q}' W^{\pm*} Z^* \rightarrow q\bar{q}' H^\pm$ [23] etc.. At the International Linear Collider (ILC) [24], H^\pm can be mainly produced in pair $e^+ e^- \rightarrow H^+ H^-$ [25] and $\gamma\gamma \rightarrow H^+ H^-$ [26] as long as kinematically accessible, and if not, single H^\pm production processes may also be useful; $e^+ e^- \rightarrow tbH^\pm$, $e^+ e^- \rightarrow \tau\nu H^\pm$ [27], $e^+ e^- \rightarrow W^\pm H^\mp$ [28–30], $\gamma\gamma(e^- \gamma) \rightarrow f\bar{f}' H^\pm$ [31, 32], etc..

In this paper, we discuss how accurately the $H^\pm W^\mp Z$ vertex can be determined at the collider experiments. At the LHC, the vertex would be determined by using the single H^\pm production from the WZ fusion[23]. The results are strongly model dependent, and the vertex may not be measured unless the H^\pm is light enough and $|\xi_\alpha|^2$ is greater than 10^{-2} . If kinematically allowed, the $H^\pm W^\mp Z$ vertex may also be measured via the decay process of $H^\pm \rightarrow W^\pm Z$ [7, 8].

We here focus on the process $e^+e^- \rightarrow W^\pm H^\mp$ at the ILC [28–30]. At the ILC, the neutral Higgs boson is produced via the Higgs strahlung process $e^+e^- \rightarrow ZH$ [33]. The mass of the Higgs boson can be determined in a model independent way by using the so-called recoil method [34], where the information of the Higgs boson can be extracted by measuring the leptonic decay products of the recoiled Z boson. In this paper we employ this method to test the $H^\pm W^\mp Z$ vertex via $e^+e^- \rightarrow W^\pm H^\mp$. We analyze the signal and backgrounds at the parton level by using CalcHEP [35]. We take into account the beam polarization and the expected resolution for the two-jet system. We find that assuming that H^\pm decays into lepton pairs, the $H^\pm W^\mp Z$ vertex can be explored accurately by measuring the signal of the two-jet with one charged lepton with missing momentum. For relatively light charged Higgs bosons, the signal significance with the value of $|\xi_\alpha|^2 \sim O(10^{-3})$ can be as large as two after appropriate kinematic cuts for the collision energy $\sqrt{s} = 300$ GeV and the integrated luminosity 1 ab^{-1} , even when the initial state radiation (ISR) is taken into account.

This paper is organized as follows. We give a quick review for the $H^\pm W^\mp Z$ vertex, and discuss the signal process $e^+e^- \rightarrow H^\pm W^\mp$ in Sec. II. The feasibility of the signal is analyzed in Sec. III. Some discussions are given in Sec. IV, and conclusions are given in Sec. V.

II. THE $H^\pm W^\mp Z$ VERTEX AND THE PROCESS $e^+e^- \rightarrow H^\pm W^\mp$

A. The $H^\pm W^\mp Z$ vertex

The $H^\pm W^\mp V$ vertex ($V = Z$ or γ) is defined in FIG. 1, where $C^{\mu\nu}$ is expressed in terms of the form factors F_{HWV} , G_{HWV} and H_{HWV} as

$$C^{\mu\nu} = F_{HWV} g^{\mu\nu} + G_{HWV} \frac{p_W^\mu p_V^\nu}{m_W^2} + iH_{HWV} \frac{p_{W\rho} p_{V\sigma}}{m_W^2} \epsilon^{\mu\nu\rho\sigma}, \quad (3)$$

with $\epsilon_{\mu\nu\rho\sigma}$ being the anti-symmetric tensor with $\epsilon_{0123} = +1$, and p_V^μ and p_W^μ being the outgoing momenta of V and W bosons, respectively. Among the form factors, $F_{HW\gamma} = 0$ is

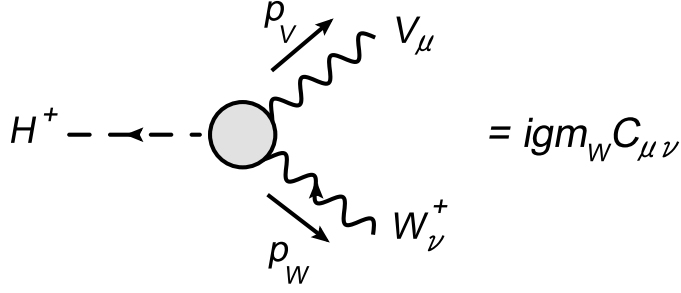


FIG. 1: The $H^{\pm}W^{\mp}V$ vertex ($V = Z$ or γ).

derived at the tree level due to the $U(1)_{\text{em}}$ gauge invariance in any extended Higgs models. These form factors F_{HWV} , G_{HWV} and H_{HWV} are respectively related to the coefficients f_{HWV} , g_{HWV} and h_{HWV} in the effective Lagrangian [7, 8];

$$\mathcal{L}_{\text{eff}} = gm_W f_{HWV} H^{\pm} W_{\mu}^{\mp} V^{\mu} + g_{HWV} H^{\pm} F_V^{\mu\nu} F_{W\mu\nu} + (ih_{HWV} \epsilon_{\mu\nu\rho\sigma} H^{\pm} F_V^{\mu\nu} F_W^{\rho\sigma} + \text{H.c.}), \quad (4)$$

where $F_V^{\mu\nu}$, and $F_W^{\mu\nu}$ are the field strengths. We note that f_{HWZ} is the coefficient of the dimension three operator, while the g_{HWV} and h_{HWV} are those of the dimension five operator, so that only f_{HWZ} may appear at the tree level. Therefore, the dominant contribution to the $H^{\pm}W^{\mp}V$ vertex is expected to be from F_{HWZ} .

In the Higgs model with only doublet scalar fields (plus singlets) all the form factors including F_{HWZ} vanish at the tree level [6], because of the custodial invariance in the kinetic term. The form factors F_{HWV} , G_{HWV} and H_{HWV} ($V = \gamma$ and Z) are generally induced at the loop level. In particular, the leading one-loop contribution to F_{HWZ} are proportional to the violation of the custodial symmetry in the sector of the particle in the loop. For example, in the two-Higgs-doublet model, the custodial symmetry is largely broken via the t - b loop contribution as well as via the Higgs sector with the mass difference between the CP-odd Higgs boson (A^0) and the charged Higgs boson H^{\pm} [8]. The one-loop induced form factors are theoretically constrained from above by perturbative unitarity [36]. In such a case, the effect of the custodial symmetry violation also can deviate the rho parameter from unity at the one loop level. However, when the lightest of CP-even neutral Higgs bosons is approximately regarded as the SM-like Higgs boson, the rho parameter can be unity even with a large mass splitting between A^0 and H^{\pm} when the masses of the heavier CP-even neutral Higgs boson H^0 and H^{\pm} are common [37]. This means that the appearance of the $H^{\pm}W^{\mp}Z$ vertex and the deviation from unity in the rho parameter are not necessarily

Model	SM with η ($Y = 0$)	SM with Δ ($Y = 1$)	the GM model
$ F_{HWZ} ^2 =$	$\frac{4v^2v_\eta^2}{\cos^2\theta_W(v^2+4v_\eta^2)^2}$	$\frac{2v^2v_\Delta^2}{\cos^2\theta_W(v^2+2v_\Delta^2)^2}$	$\frac{4v_\Delta^2}{\cos^2\theta_W(v^2+4v_\Delta^2)}$
$\rho_{\text{tree}} =$	$1 + \frac{4v_\eta^2}{v^2}$	$\frac{1+2\frac{v_\Delta^2}{v^2}}{1+4\frac{v_\Delta^2}{v^2}}$	1

TABLE I: The tree-level expression for F_{HWZ} and rho parameter at the tree level in the model with a real triplet field, that with a complex triplet field and the Georgi-Machacek (GM) model [13].

correlated at the one-loop level, and they can be independent quantities, in principle.

The simplest models in which the $H^\pm W^\mp Z$ vertex appears at the tree level are those with triplet scalar fields. In the model with an isospin doublet field ($Y = 1/2$) and either an real triplet field η ($Y = 0$) or an additional complex triplet field Δ ($Y = 1$), concrete expressions for the tree-level formulae for $|F_{HWZ}|^2$ and that of ρ_{tree} are shown in TABLE I, where v , v_η and v_Δ are respectively VEVs of the doublet scalar field and the additional triplet scalar field η and Δ . These triplet scalar fields also contribute to the rho parameter at the tree level, so that their VEVs are constrained by the current rho parameter data, $\rho_{\text{exp}} = 1.0008^{+0.0017}_{-0.0007}$; i.e., $v_\eta \lesssim 6$ GeV for the real triplet field η , and $v_\Delta \lesssim 8$ GeV for the complex triplet Δ (95 % CL). We note that in order to obtain the similar accuracy to the rho parameter data by measuring the $H^\pm W^\mp Z$ vertex, the vertex has to be measured with the detectability to $|F_{HWZ}|^2 \sim \mathcal{O}(10^{-3})$.

Finally, we mention about the model with a real triplet field η and a complex triplet field Δ in addition to the SM, which is proposed by Georgi-Machacek and Chanowiz-Golden [13–15]. In this model, an alignment of the VEVs for η and Δ are introduced ($v_\eta = v_\Delta/\sqrt{2}$), by which the Higgs potential is invariant under the custodial $SU(2)$ symmetry at the tree level. Physical scalar states in this model can be classified using the transformation property against the custodial symmetry; i.e., the five-plet, the three-plet and the singlet. Only the charged Higgs boson from the five-plet state has the non-zero value of F_{HWZ} at the tree level. Its value is proportional to the VEV v_Δ for the triplet scalar fields. However, the value of v_Δ is not strongly constrained by the rho parameter data, because the tree level contribution to the rho parameter is zero due to the custodial symmetry: see TABLE I. Consequently, the magnitude of $|F_{HWZ}|^2$ can be of order one.

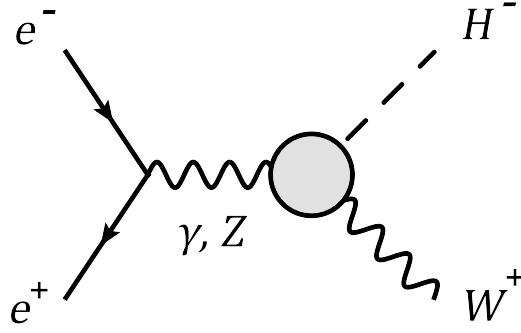


FIG. 2: The $e^+e^- \rightarrow H^-W^+$ process

B. The $e^+e^- \rightarrow H^\pm W^\mp$ process

The process $e^+e^- \rightarrow H^-W^+$ is depicted in FIG. 2. This process is directly related to the $H^\pm W^\mp Z$ vertex. The helicity amplitudes are calculated by

$$\mathcal{M}(\tau, \lambda) = \sum_{V=Z, \gamma} igm_W C_V \frac{1}{s - m_V^2} j_\mu(\tau) C^{\mu\nu} \epsilon_\nu(\lambda), \quad (5)$$

where \sqrt{s} is the center-of-mass energy, $j_\mu(\tau)$ is the electron current, and $\epsilon_\nu(\lambda)$ is the polarization vector of the W^+ boson [29]. The helicities of the electron and the W^+ boson can be $\tau = \pm 1$ and $\lambda = 0, \pm 1$, respectively. The coefficient C_V is given by

$$C_V = \begin{cases} eQ_e, & \text{for } V = \gamma, \\ \frac{g}{\cos \theta_W} (T_e^3 - \sin^2 \theta_W Q_e), & \text{for } V = Z, \end{cases} \quad (6)$$

with $Q_e = -1$, $T_e^3 = -1/2$ (0) for $\tau = -1$ ($+1$). The squared amplitude is evaluated as

$$\begin{aligned} |\mathcal{M}(\tau)|^2 &\equiv \sum_{\lambda=0, \pm} |\mathcal{M}(\tau, \lambda)|^2 \\ &= g^2 \left| C_\gamma \frac{F_{HW\gamma}}{s} + C_Z \frac{F_{HWZ}}{s - m_Z^2} \right|^2 \left[\frac{\sin^2 \theta}{4} (s + m_W^2 - m_{H^\pm}^2)^2 + sm_W^2 (\cos^2 \theta + 1) \right], \end{aligned} \quad (7)$$

where θ is the angle between the momentum of H^\pm and the beam axis, m_{H^\pm} is the mass of H^\pm and the form factors G_{HWV} and H_{HWV} are taken to be zero. The helicity specified cross sections are written in terms of the squared amplitude in Eq. (7),

$$\sigma(s; \tau) = \frac{1}{32\pi s} \beta \left(\frac{m_{H^\pm}^2}{s}, \frac{m_W^2}{s} \right) \int_{-1}^1 d\cos \theta |\mathcal{M}(\tau)|^2, \quad (8)$$

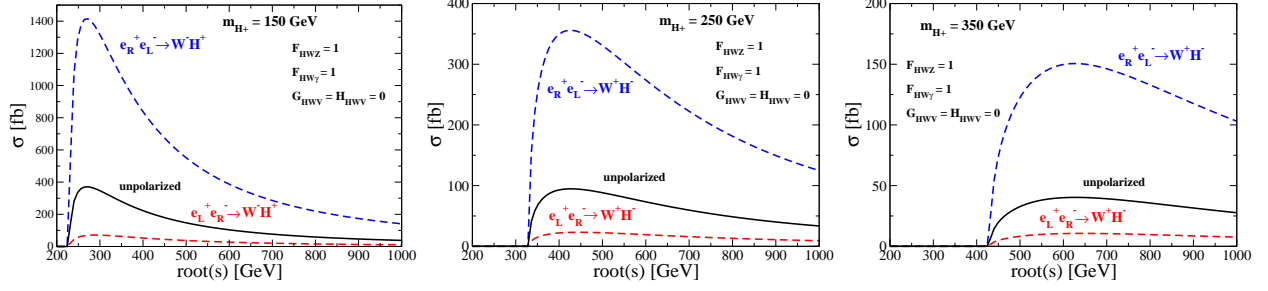


FIG. 3: The total cross section as a function of \sqrt{s} in the case of $F_{HWZ} = F_{HW\gamma} = 1$.

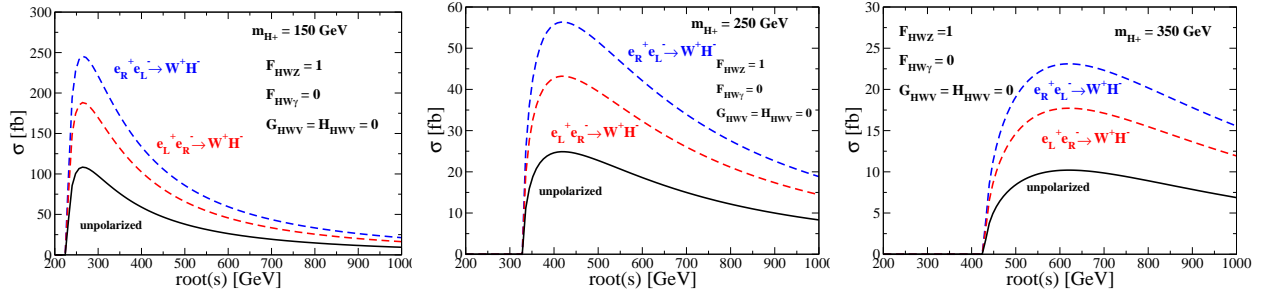


FIG. 4: The total cross section as a function of \sqrt{s} in the case of $F_{HWZ} = 1, F_{HW\gamma} = 0$.

where $\sigma(s; +1) = \sigma(e_L^+ e_R^- \rightarrow H^- W^+)$ and $\sigma(s; -1) = \sigma(e_R^+ e_L^- \rightarrow H^- W^+)$, and

$$\beta(x, y) = \sqrt{1 + x^2 + y^2 - 2xy - 2x - 2y}. \quad (9)$$

The helicity averaged cross section is given by $\sigma(e^+ e^- \rightarrow H^- W^+) = (\sigma(s, +1) + \sigma(s, -1))/4$.

In FIGs. 3 and 4, we show that the \sqrt{s} dependence of the helicity dependent and the helicity averaged cross sections. Notice that the behavior of these cross sections drastically changes depending on the initial electron helicity in the case of $F_{HWZ} \simeq F_{HW\gamma}$. On the contrary, there is no such a difference in the case of $F_{HWZ} \gg F_{HW\gamma}$. As mentioned before, $F_{HW\gamma}$ is zero at the tree level in any models because of the $U(1)_{\text{em}}$ gauge invariance. The relation of $F_{HWZ} \gg F_{HW\gamma}$ or $F_{HWZ} \simeq F_{HW\gamma}$ can be tested by using the initial electron helicities.

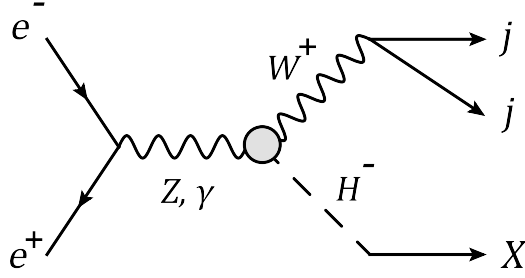


FIG. 5: The signal process.

III. THE SIGNAL AND BACKGROUND ANALYSIS

A. Recoil method and the assumption for the ILC performance

We investigate the possibility of measuring the $H^\pm W^\mp Z$ vertex by using a recoil method at the ILC. It has been known that this method is a useful tool for measuring the mass of the SM-like Higgs boson H_{SM} without assuming the decay branching fraction of the Higgs boson [34]. In the Higgs-strahlung process $e^+e^- \rightarrow ZH_{\text{SM}}$ [33], the Higgs boson mass can be obtained as the recoil mass m_{recoil} from two leptons produced from the Z boson, whose energy is $E_{\ell\ell}$, and the invariant mass is $M_{\ell\ell}$. They satisfy the relation,

$$m_{\text{recoil}}^2(\ell\ell) = s - 2\sqrt{s}E_{\ell\ell} + M_{\ell\ell}^2. \quad (10)$$

The information of the Higgs boson mass can be extracted by measuring $E_{\ell\ell}$ and $m_{\ell\ell}$ in a model independent way.

In this paper we apply this method to $e^+e^- \rightarrow W^\pm H^\mp$ in order to measure the $H^\pm W^\mp Z$ vertex. In order to identify the process, we consider the hadronic decays $W \rightarrow jj$ instead of the leptonic decay of the produced W boson, and obtain information of the $H^\pm W^\mp Z$ vertex by using the recoil of the two-jet system. The recoiled mass of H^\pm is given in terms of the two-jet energy E_{jj} and the two-jet invariant mass M_{jj} as

$$m_{\text{recoil}}^2(jj) = s - 2\sqrt{s}E_{jj} + M_{jj}^2. \quad (11)$$

This process is shown in FIG. 5. It is clear that the detector performance for the resolution of two jets is crucial in such an analysis. In particular, the jets from the W boson in the signal process has to be precisely measured in order to be separated with those from the Z

boson in the background process. At the ILC, the resolution for the two jet system with the energy E in the unit of GeV is expected to be $\sigma_E = 0.3\sqrt{E}$ GeV, by which the background from $Z \rightarrow jj$ can be considerably reduced. We here adopt the similar value for σ_E (~ 3 GeV) in our later analysis.

At the ILC, the polarized electron and positron beams can be used, by which the background from the W boson pair production process can be reduced. We here use the following beams polarized as

$$\frac{N_{e_R^-} - N_{e_L^-}}{N_{e_L^-} + N_{e_R^-}} = 0.8, \quad \frac{N_{e_L^+} - N_{e_R^+}}{N_{e_L^+} + N_{e_R^+}} = 0.5, \quad (12)$$

which are expected to be attained at the ILC [24], where $N_{e_{R,L}^-}$ and $N_{e_{R,L}^+}$ are numbers of right- (left-) handed electron and positron in the beam flux per unit time. The total cross sections for the signal and the backgrounds can be evaluated from the helicity specified cross sections as

$$\begin{aligned} \sigma_{\text{tot}}(e^+e^- \rightarrow X) = & x_-x_+\sigma(e_L^+e_R^- \rightarrow X) + (1-x_-)(1-x_+)\sigma(e_R^+e_L^- \rightarrow X) \\ & + x_-(1-x_+)\sigma(e_R^+e_R^- \rightarrow X) + x_+(1-x_-)\sigma(e_L^+e_L^- \rightarrow X), \end{aligned} \quad (13)$$

where $x_- = N_{e_R^-}/(N_{e_L^-} + N_{e_R^-})$ and $x_+ = N_{e_L^+}/(N_{e_L^+} + N_{e_R^+})$.

The high-energy electron and positron beams lose their incident energies by the ISR. In our analysis, we also take into account such effect, and see how the results without the ISR are changed by including the effect of the ISR.

B. Signal and Backgrounds

The size of the signal cross section is determined by the center of mass energy \sqrt{s} , the mass m_{H^\pm} and the form factors F_{HWZ} and $F_{HW\gamma}$. In the following analysis, we consider the case of $(F_{HWZ}, F_{HW\gamma}) \equiv (\xi, 0)$. This approximately corresponds to most of the cases we are interested, such as the triplet models. In order to examine the possibility of constraining $|\xi|^2$, we here assume that the mass of the charged Higgs boson is already known with some accuracy by measuring the other processes at the LHC or at the ILC. Then $|\xi|^2$ is a unique free parameter in the production cross section.

In order to perform the signal and background analysis, we here assume that the decay of the produced charged Higgs boson is lepton specific; i.e., $H^\pm \rightarrow \ell\nu$ where ℓ is either e ,

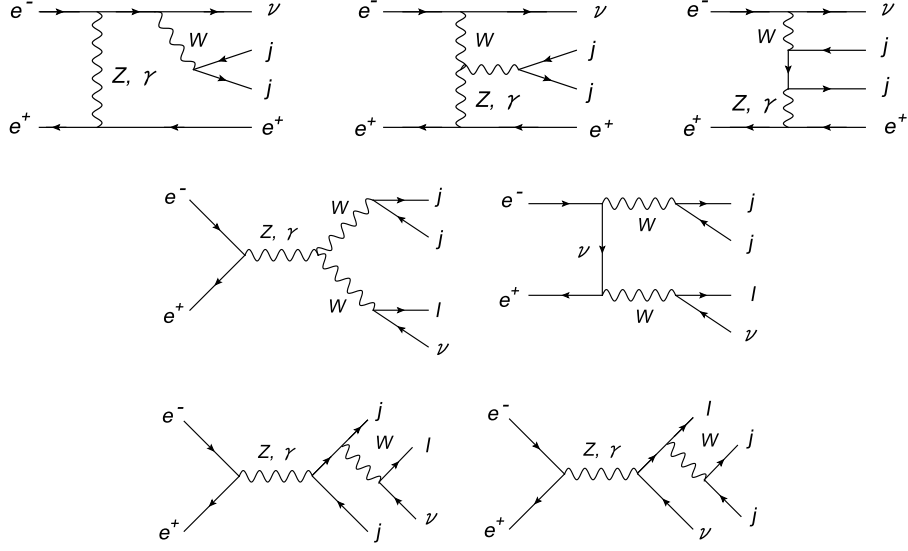


FIG. 6: The $e^+e^- \rightarrow \ell \nu jj$ backgrounds.

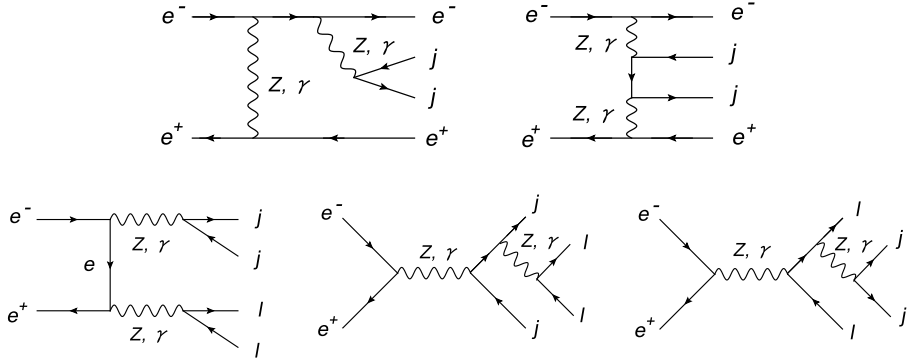


FIG. 7: The $e^+e^- \rightarrow \ell \ell jj$ backgrounds.

μ or τ . The final state of the signal is then $e^+e^- \rightarrow H^\pm W^\mp \rightarrow \ell \nu jj$. We first consider $m_{H^\pm} < m_W + m_Z$ to avoid the complexness with the possible decay mode of $H^\pm \rightarrow W^\pm Z$, whose branching ratio strongly depends on the model. The main backgrounds come from the W boson pair production process $e^+e^- \rightarrow W^+W^-$ and the single W production processes in FIG. 6. For the $e^\pm \nu jj$ final state, additional processes shown in FIG. 6 (upper figures) can also be a significant background. In addition, we take into account the processes with the final state of $\ell \ell jj$ shown in FIG. 7. They can be backgrounds if one of the outgoing leptons escapes from the detection at the detector. We here assume that the miss identity rate for a lepton is 10 %.

We impose the basic cuts for all events such as

$$10^\circ < A_j < 170^\circ, \quad 5^\circ < A_{jj} < 175^\circ, \quad 10 \text{ GeV} < E_{jj}, \quad (14)$$

where A_j is the angle between a jet and the beam axis, A_{jj} is the angle between the two jets and E_{jj} is the energy of the two jets. In the numerical evaluation, we use CalcHEP [35].

After the basic cuts, the event numbers of both the signal and the backgrounds are listed in TABLE II for the case without ISR, and in TABLE III for that with ISR, where the center of mass energy is set $\sqrt{s} = 300 \text{ GeV}$, the mass of the charged Higgs boson m_{H^\pm} is 150 GeV, and the parameter $|\xi|^2$ for the $H^\pm W^\mp Z$ vertex is set to be 10^{-3} . For both the cases signal over background ratios are less than 10^{-4} before imposing the other kinematic cuts than the basic cuts in Eq. (14). In the following we first discuss the case without the ISR, then present the results for that with the ISR.

In order to improve the signal over background ratio, we impose additional kinematic cuts. The two jets come from the W boson for the signal, so that the invariant mass cut is useful to reduce the backgrounds where a parent of the two jets is not the W boson. We here impose the condition;

$$m_W - n\sigma_E < M_{jj} < m_W + n\sigma_E, \quad (15)$$

where σ_E represents the resolution of the detector which we assume 3 GeV, and n is taken to be 2 here.

In FIG. 8, the differential cross sections of the signal and the backgrounds are shown for the events after the M_{jj} cut in Eq. (15) as a function of the transverse momentum p_T^{jj} , the energy of the jj system, the angle θ_{lep} of a charged lepton with the beam axis, and the invariant mass $M_{\ell\nu}$ of the charged lepton and the missing momentum in the final state. For the signal, the results are shown for $|\xi|^2 = 1$ with the mass of the charged Higgs boson to be 110, 130, 150 and 170 GeV. The E_{jj} distribution shown in FIG. 8 (upper-right) can be translated into the distribution as a function of m_{recoil} by using the relation in Eq. (11), which is shown in FIG. 9. The signal events form the peak at $m_{\text{recoil}} \sim m_{H^\pm}$.

According to FIG. 8, we impose the following four kinematic cuts sequentially:

$$75 \text{ GeV} < p_T^{jj} < 100 \text{ GeV}, \quad (16)$$

and

$$115 \text{ GeV} < E_{jj} < 125 \text{ GeV} \quad (17)$$

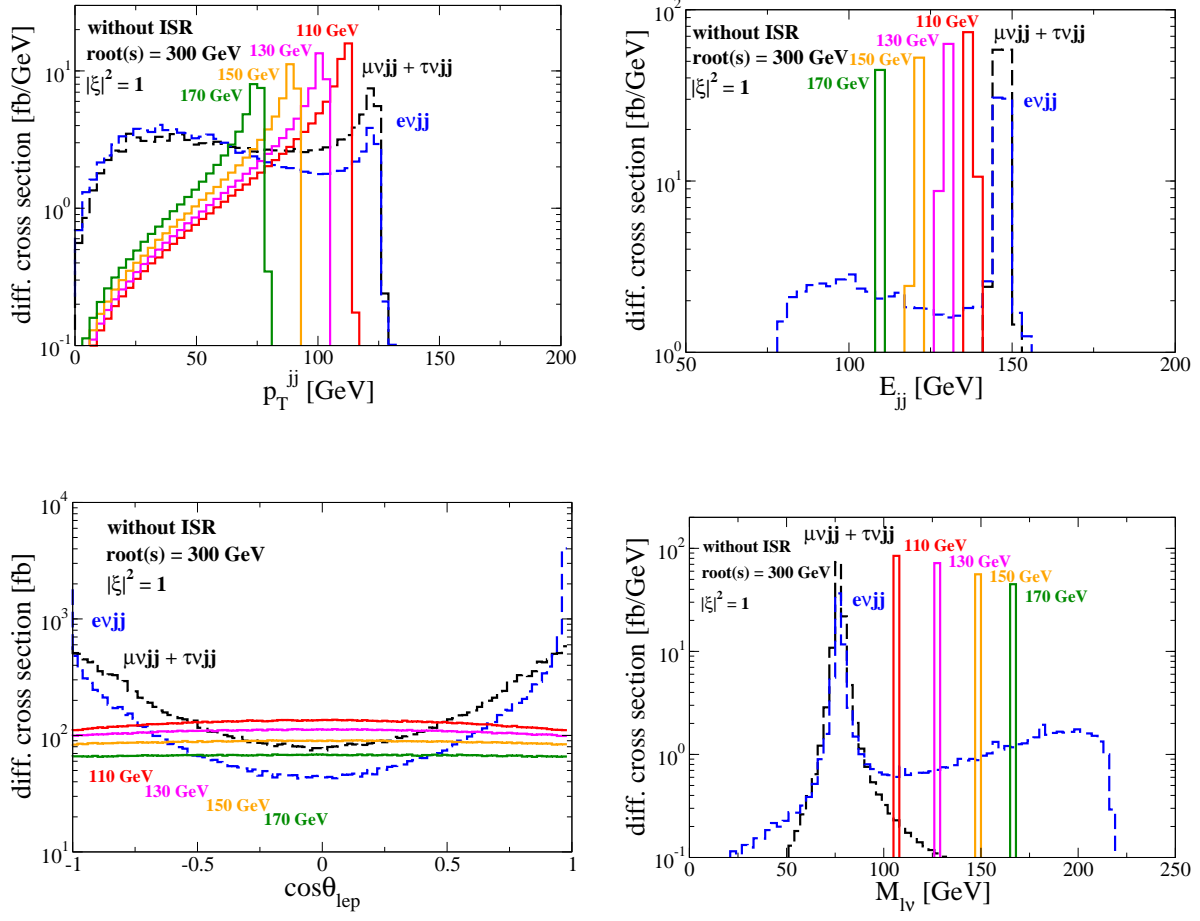


FIG. 8: Distributions of the signal for $m_{H^\pm} = 110, 130, 150$ and 170 GeV as well as the backgrounds after the invariant mass M_{jj} cut in Eq. (15) without the ISR as a function of the transverse momentum p_T^{jj} (upper left), the energy of the jj system (upper right), the angle θ_{lep} of a charged lepton with the beam axis (lower left), and the invariant mass $M_{l\nu}$ of the charged lepton and the missing momentum in the final state (lower right). $|\xi|^2$ is taken to be 1.

for the jj system in the final state. In TABLE II, the resulting values for the cross sections for the signal and backgrounds are shown in each step of the cuts. The backgrounds can be reduced in a considerable extent. For $|\xi|^2 = 10^{-3}$, the signal significance reaches to $\mathcal{O}(1)$ assuming the integrated luminosity of 1 ab^{-1} .

Until now, we have imposed the cuts on the jj system, and no information from the $\ell\nu$ system has been used. Here, in order to further improve the signal significance, we impose

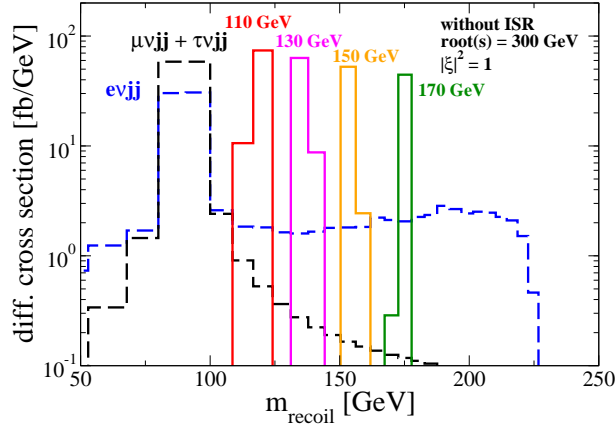


FIG. 9: Distributions of the signal for $m_{H^\pm} = 110, 130, 150$ and 170 GeV as well as the backgrounds after the cut in Eq. (15) without the ISR as a function of the recoil mass m_{recoil} .

new cuts related to the $\ell\nu$ system in order, which are determined from FIG. 8;

$$|\cos \theta_{\text{lep}}| < 0.75, \quad (18)$$

and

$$144 \text{ GeV} < M_{\ell\nu} < 156 \text{ GeV}. \quad (19)$$

As shown in TABLE II, for $|\xi|^2 = 10^{-3}$ the signal significance after these cuts can reach to $S/\sqrt{B} \simeq 2.5$ and the signal over background ratio can be $S/B \sim 10\%$, assuming the integrated luminosity of 1 ab^{-1} .

Next let us see how this results can be changed by including the ISR. The beam parameters at $\sqrt{s} = 500$ GeV are given in Ref. [24], such as the bunch $x + y$ size, the bunch length and the number of particles per a bunch. We here use the default values defined in CalcHEP [35]; i.e., the bunch $x + y$ size = 560 nm , bunch length = $400 \mu\text{m}$, and the number of particles/bunch = 2×10^{10} at $\sqrt{s} = 300 \text{ GeV}$ ¹.

In FIG. 10, the similar distributions to those in FIG. 8 but with the ISR are given for the signal and the backgrounds after the invariant mass M_{jj} cut in Eq. (15). The biggest change can be seen in the E_{jj} distribution. The background events originally located at the point just below 150 GeV in the case without the ISR, which corresponds to the W boson mass,

¹ We have confirmed that the results are almost unchanged even when we use the values given in Ref. [24].

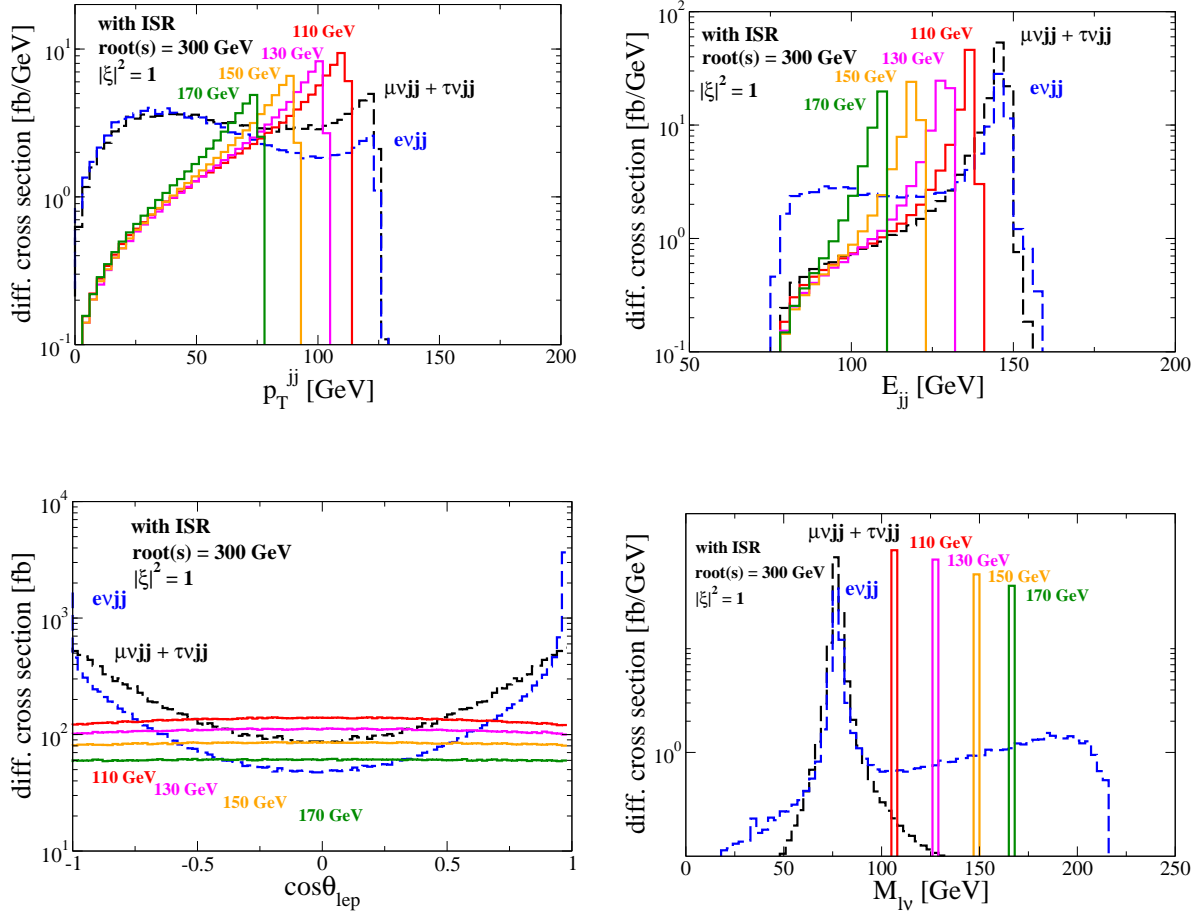


FIG. 10: Distributions of the signal for $m_{H^\pm} = 110, 130, 150$ and 170 GeV as well as the backgrounds after the invariant mass M_{jj} cut in Eq. (15) with the ISR as a function of the transverse momentum p_T^{jj} (upper left), the energy of the jj system (upper right), the angle θ_{lep} of a charged lepton with the beam axis (lower left), and the invariant mass $M_{\ell\nu}$ of the charged lepton and the missing momentum in the final state (lower right). $|\xi|^2$ is taken to be 1.

tend to move in the lower E_{jj} regions, so that the signal over background ratio becomes worse. The recoil mass distribution is shown in FIG. 11.

Consequently, the signal significance after all the cuts is smeared from 2.5 to 2.0, while the signal over background ratio is changed from 8.7×10^{-2} to 7.5×10^{-2} . Cross sections of the signal and the backgrounds with the ISR are listed in TABLE III with the values of S/\sqrt{B} and S/B for each stage of kinematic cuts. We stress that even taking the ISR into account, the $H^\pm W^\mp Z$ vertex with $|\xi|^2 > 10^{-3}$ can be excluded with 95% CL.

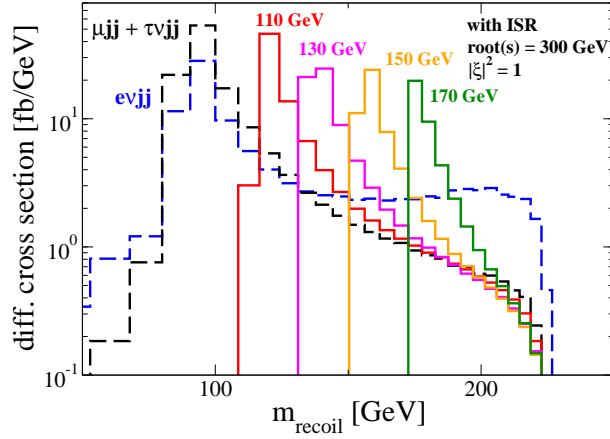


FIG. 11: Distributions of the signal for $m_{H^\pm} = 110, 130, 150$ and 170 GeV as well as the backgrounds after the cut in Eq. (15) with the ISR as a function of the recoil mass m_{recoil} .

IV. DISCUSSIONS

In the above analysis, we have not distinguished differences among the charged leptons $\ell^\pm = e^\pm, \mu^\pm$ and τ^\pm . Although we have assumed that the H^\pm decay is lepton specific, the branching ratios of $H^\pm \rightarrow e^\pm \nu, \mu^\pm \nu$ and $\tau^\pm \nu$ depend on details of each Higgs model. For example, in the type II seesaw model [38], the decay pattern of H^\pm is related to the neutrino mass and mixing. Once we assume the decay pattern, we can easily estimate the signal significance by using TABLE II or III for each specific model. If H^\pm mainly decays into $e^\pm \nu$, the final state is $e\nu jj$. The backgrounds become 70 % of all the $\ell\nu jj$ backgrounds as evaluated from TABLE III, while the signal is unchanged. The S/\sqrt{B} becomes about 2.4 with taking into account the ISR. If H^\pm mainly decays into $\mu^\pm \nu$, we consider the $\mu\nu jj$ final state. In this case, the number of the signal event is unchanged while that of the background becomes 15 % of all the $\ell\nu jj$ backgrounds, so that the S/\sqrt{B} is expected to be multiplied by about 2.5 for the case with ISR; i.e., $S/\sqrt{B} \sim 5$ for $|\xi|^2 = 10^{-3}$. On the contrary, if H^\pm mainly decays into $\tau^\pm \nu$, the $\tau\nu jj$ backgrounds 15 % of all the $\ell\nu jj$ backgrounds. However, the efficiency for τ^\pm has to be multiplied so that it would become worse than that for μ^\pm .

In extended Higgs sectors, there can be additional backgrounds which is relevant to the other scalar bosons than H^\pm . For example, if one of the neutral Higgs bosons H has the similar mass to that of H^\pm , then the process $e^+e^- \rightarrow ZH \rightarrow \ell\ell jj$ (or $jj\ell\ell$) can be the background. In this case, its contribution is expected to be reduced by the kinematic cut

of M_{jj} in Eq. (15) with the good resolution of the ILC ($\sigma_E \sim 0.3\sqrt{E}$ GeV). Also, the rate of missing one of the charged leptons has to be multiplied. The change of signal significance cannot be expected to be dominant. As the second example, we mention about pair production of doubly charged Higgs bosons $e^+e^- \rightarrow H^{++}H^{--} \rightarrow \ell^+\ell^+\ell^-\ell^-$ with the similar mass to that of H^\pm . Such degenerate masses between H^\pm and $H^{\pm\pm}$ may often happen in the models with triplets. When the final state is of four charged leptons, we can reduce such a background by imposing the veto for three or four leptons in the final state.

Finally, we comment on the case where H^\pm is relatively heavy as compared to the value we have assumed above. When $m_{H^\pm} > m_W + m_Z$, the main decay mode of H^\pm may be WZ , instead of $\ell\nu$. The final state of the signal would be $\ell\nu jjjj$, $\ell\ell\nu\nu jj$ or $\ell\ell jjjj$, so that the analysis should be different from the $\ell\nu jj$ final state. It is expected that the signal significance for such a case would become rather worse. Furthermore, when $m_{H^\pm} > 2m_t$, the $t\bar{t}$ pair production mode becomes additional background. In order to clarify the feasibility of the $H^\pm W^\mp Z$ vertex for such a case, we need to proceed to the analysis for such final states, but this is beyond the scope of our paper.

V. CONCLUSIONS

We have discussed the possibility of measuring the $H^\pm W^\mp Z$ vertex at the ILC. The vertex is important to understand the exoticness of the Higgs sector, so that the combined information of this vertex with the rho parameter provides a useful criterion to determine the structure of the extended Higgs sector. Assuming that the decay of the charged Higgs bosons is lepton specific, which is natural for the exotic representations of the extra scalar bosons, the feasibility of the vertex is analyzed by using the recoil method via the process $e^+e^- \rightarrow H^\pm W^\mp \rightarrow \ell\nu jj$ with the parton level simulation for the background reduction. We have found that the vertex with $|F_{HWZ}|^2 \geq \mathcal{O}(10^{-3})$ can be excluded with the 95% confidence level when $120\text{-}130 \text{ GeV} < m_{H^\pm} < m_W + m_Z$. For heavier charged Higgs bosons, the decay into WZ may be dominant so that the analysis becomes model dependent. The measurement of the $H^\pm W^\mp Z$ vertex with $|F_{HWZ}|^2 \geq \mathcal{O}(10^{-3})$ gives a precise information for the Higgs sector, whose accuracy is similar to that of the rho parameter. In conclusion, the measurement of the $H^\pm W^\mp Z$ vertex at the ILC is therefore very interesting, and give a motivation to perform the more realistic detector level simulation.

Acknowledgments

The authors would like to thank Hitoshi Yamamoto and Keisuke Fujii for useful discussions and comments. The work of SK was supported in part by Grant-in-Aid for Scientific Research (A) no. 22244031 and (C) no. 19540277, that of KY was supported by Japan Society for the Promotion of Science (JSPS Fellow (DC2)).

- [1] K. Nakamura, et al., (Particle Data Group), J. Phys. G **37**, 075021 (2010).
- [2] J. F. Gunion, H. E. Haber, G. L. Kane and S. Dawson, “THE HIGGS HUNTER’S GUIDE,” Front. Phys. **80**, 1 (2000).
- [3] E. Gildener and S. Weinberg, Phys. Rev. D **13**, 3333 (1976).
- [4] J. Alcaraz *et al.* [ALEPH and DELPHI and L3 and OPAL and LEP Electroweak Working Group Collaborations], [hep-ex/0612034].
- [5] M. E. Peskin and T. Takeuchi, Phys. Rev. Lett. **65**, 964 (1990); Phys. Rev. D **46**, 381 (1992).
- [6] J. A. Grifols and A. Mendez, Phys. Rev. D **22**, 1725 (1980); A.A. Iogansen, N.G. Uraltsev, V.A. Khoze, *Sov. J. Nucl. Phys.* **36** (1982) 717.
- [7] A. Mendez and A. Pomarol, Nucl. Phys. B **349**, 369 (1991); M. C. Peyranere, H. E. Haber and P. Irulegui, Phys. Rev. D **44**, 191 (1991); J.L. Díaz-Cruz, J. Hernández-Sánchez, J.J. Toscano, Phys. Lett. B **512**, 339 (2001).
- [8] S. Kanemura, Phys. Rev. D **61**, 095001 (2000).
- [9] H. Haber, H. Logan, Phys. Rev. D **62**, 015011 (2000).
- [10] S. L. Glashow and S. Weinberg, Phys. Rev. D **15**, 1958 (1977).
- [11] V. D. Barger, J. L. Hewett and R. J. N. Phillips, Phys. Rev. D **41**, 3421 (1990); Y. Grossman, Nucl. Phys. B **426**, 355 (1994).
- [12] M. Aoki, S. Kanemura, K. Tsumura and K. Yagyu, Phys. Rev. D **80**, 015017 (2009); H. S. Goh, L. J. Hall and P. Kumar, JHEP **0905**, 097 (2009); S. Su and B. Thomas, Phys. Rev. D **79**, 095014 (2009); H. E. Logan and D. MacLennan, Phys. Rev. D **79**, 115022 (2009).
- [13] H. Georgi and M. Machacek, Nucl. Phys. B **262**, 463 (1985); M. S. Chanowitz and M. Golden, Phys. Lett. B **165**, 105 (1985).
- [14] J. F. Gunion, R. Vega and J. Wudka, Phys. Rev. D **42**, 1673 (1990); R. Vega and D. A. Dicus, Nucl. Phys. B **329**, 533 (1990). J. F. Gunion, R. Vega and J. Wudka, Phys. Rev. D **43**, 2322

- (1991); R. Godbole, B. Mukhopadhyaya and M. Nowakowski, Phys. Lett. B **352**, 388 (1995).
- [15] M. Aoki and S. Kanemura, Phys. Rev. D **77**, 095009 (2008); H. E. Logan, M. -A. Roy, Phys. Rev. **D82**, 115011 (2010). [arXiv:1008.4869 [hep-ph]].
- [16] A. C. Bawa, C. S. Kim and A. D. Martin, Z. Phys. C **47** (1990) 75;
- [17] J. F. Gunion, H. E. Haber, F. E. Paige, W. K. Tung and S. S. D. Willenbrock, Nucl. Phys. B **294**, 621 (1987).
- [18] D. A. Dicus, J. L. Hewett, C. Kao and T. G. Rizzo, Phys. Rev. D **40** (1989) 787; A. A. Barrientos Bendezú and B. A. Kniehl, Phys. Rev. D **59** (1999) 015009; *ibid.* D **61** (2000) 097701; *ibid.* D **63** (2001) 015009; O. Brein, W. Hollik and S. Kanemura, Phys. Rev. D **63** (2001) 095001; Y. S. Yang, C. S. Li, L. G. Jin and S. H. Zhu, Phys. Rev. D **62** (2000) 095012; F. Zhou, W. G. Ma, Y. Jiang, L. Han and L. H. Wan, Phys. Rev. D **63** (2001) 015002; W. Hollik and S. H. Zhu, Phys. Rev. D **65** (2002) 075015; E. Asakawa, O. Brein and S. Kanemura, Phys. Rev. D **72**, 055017 (2005); D. Eriksson, S. Hesselbach, J. Rathsmann, Eur. Phys. J. **C53**, 267-280 (2008).
- [19] S. Willenbrock, Phys. Rev. D **35**, 173 (1987); O. Brein and W. Hollik, Eur. Phys. J. C **13**, 175 (2000); A.A. Barrientos Bendezu and B.A. Kniehl, Phys. Rev. D **64**, 035006 (2001).
- [20] E. Eichten, I. Hinchliffe, K. D. Lane and C. Quigg, Rev. Mod. Phys. **56**, 579 (1984) [Addendum-*ibid.* **58**, 1065 (1986)].
- [21] S. Kanemura and C. P. Yuan, Phys. Lett. B **530**, 188 (2002); Q. H. Cao, S. Kanemura and C. P. Yuan, Phys. Rev. D **69**, 075008 (2004); A. Belyaev, Q. -H. Cao, D. Nomura, K. Tobe, C. -P. Yuan, Phys. Rev. Lett. **100**, 061801 (2008).
- [22] A. G. Akeroyd, M. Aoki, Phys. Rev. **D72**, 035011 (2005).
- [23] E. Asakawa and S. Kanemura, Phys. Lett. B **626**, 111 (2005); E. Asakawa, S. Kanemura and J. Kanzaki, Phys. Rev. D **75**, 075022 (2007); M. Battaglia, A. Ferrari, A. Kiiskinen, T. Maki, [hep-ex/0112015]; S. Godfrey, K. Moats, Phys. Rev. **D81**, 075026 (2010).
- [24] J. Brau, (Ed.) *et al.* [ILC Collaboration], [arXiv:0712.1950 [physics.acc-ph]]; G. Aarons *et al.* [ILC Collaboration], [arXiv:0709.1893 [hep-ph]]; T. Behnke, (Ed.) *et al.* [ILC Collaboration], [arXiv:0712.2356 [physics.ins-det]].
- [25] S. Komamiya, Phys. Rev. D **38**, 2158 (1988); A. Djouadi, J. Kalinowski, P. Ohmann, P. M. Zerwas, Z. Phys. **C74**, 93-111 (1997); A. Kiiskinen, P. Poyhonen, M. Battaglia, [hep-ph/0101239]; J. Guasch, W. Hollik, A. Kraft, Nucl. Phys. **B596**, 66-80 (2001).

- [26] D. Bowser-Chao, K. -m. Cheung, S. D. Thomas, Phys. Lett. **B315**, 399-405 (1993).
- [27] S. Kanemura, S. Moretti and K. Odagiri, JHEP **0102**, 011 (2001).
- [28] K. Cheung, R. J. N. Phillips and A. Pilaftsis, Phys. Rev. D **51**, 4731 (1995).
- [29] S. Kanemura, Eur. Phys. J. C **17**, 473 (2000).
- [30] S.-H. Zhu, hep-ph/9901221; A. Arhrib, et al., Nucl. Phys. B **581**, 34 (2000); H.E. Logan, S. Su, Phys. Rev. D **66**, 035001 (2002); Phys. Rev. D **67**, 017703, (2003); K. Cheung, R. Phillips, A. Pilaftsis, Phys. Rev. D **51**, 4731 (1995); R.M. Godbole, B. Mukhopadhyaya, M. Nowakowski, Phys. Rev. D **352**, 388 (1995); D.K. Ghosh, R.M. Godbole, B. Mukhopadhyaya, Phys. Rev. D **55**, 3150 (1997).
- [31] H. J. He, S. Kanemura and C. P. Yuan, Phys. Rev. Lett. **89**, 101803 (2002); H. J. He, S. Kanemura and C. P. Yuan, Phys. Rev. D **68**, 075010 (2003); S. Moretti and S. Kanemura, Eur. Phys. J. C **29**, 19 (2003).
- [32] S. Kanemura, S. Moretti and K. Odagiri, Eur. Phys. J. C **22**, 401 (2001).
- [33] J. R. Ellis, M. K. Gaillard, D. V. Nanopoulos, Nucl. Phys. **B106**, 292 (1976); J. D. Bjorken, SLAC Report, 198 (1976); B. L. Ioffe, V. A. Khoze, Sov. J. Part. Nucl. **9**, 50 (1978); D. R. T. Jones, S. T. Petcov, Phys. Lett. **B84**, 440 (1979).
- [34] W. Lohmann, M. Ohlerich, A. Raspereza and A. Schalicke, *In the Proceedings of 2007 International Linear Collider Workshop (LCWS07 and ILC07), Hamburg, Germany, 30 May - 3 Jun 2007, pp TIG13* [arXiv:0710.2602 [hep-ex]]; H. Li, F. Richard, R. Poeschl and Z. Zhang, arXiv:0901.4893 [hep-ex].
- [35] A. Pukhov, [hep-ph/0412191].
- [36] S. Kanemura, T. Kubota and E. Takasugi, Phys. Lett. B **313**, 155 (1993); A. G. Akeroyd, A. Arhrib, E. -M. Naimi, Phys. Lett. **B490**, 119-124 (2000). I. F. Ginzburg and I. P. Ivanov, Phys. Rev. D **72**, 115010 (2005).
- [37] H. E. Haber, A. Pomarol, Phys. Lett. **B302**, 435-441 (1993); A. Pomarol, R. Vega, Nucl. Phys. **B413**, 3-15 (1994).
- [38] J. Schechter and J. W. F. Valle, Phys. Rev. D **22** (1980) 2227; T. P. Cheng and L. F. Li, Phys. Rev. D **22** (1980) 2860; M. Magg and C. Wetterich, Phys. Lett. B **94** (1980) 61; C. Wetterich, Nucl. Phys. B **187** (1981) 343; G. Lazarides, Q. Shafi and C. Wetterich, Nucl. Phys. B **181** (1981) 287; R. N. Mohapatra and G. Senjanovic, Phys. Rev. D **23** (1981) 165.

	Basic	M_{jj}	p_T^{jj}	E_{jj}	$\cos \theta_{\text{lep}}$	$M_{\ell\nu}$
$e_R^+ e_L^- \rightarrow \ell^\pm \nu jj$ (fb)	7.2×10^{-3}	6.4×10^{-3}	4.4×10^{-3}	4.4×10^{-3}	3.3×10^{-3}	3.3×10^{-3}
$e_L^+ e_R^- \rightarrow \ell^\pm \nu jj$ (fb)	1.4×10^{-1}	1.3×10^{-1}	8.5×10^{-2}	8.5×10^{-2}	6.7×10^{-2}	6.7×10^{-2}
Total signal (fb)	1.5×10^{-1}	1.4×10^{-1}	8.9×10^{-2}	8.9×10^{-2}	7.0×10^{-2}	7.0×10^{-2}
$e_R^+ e_L^- \rightarrow \mu^\pm \nu jj + \tau^\pm \nu jj$ (fb)	340	300	53	2.9×10^{-1}	2.2×10^{-1}	1.3×10^{-1}
$e_L^+ e_R^- \rightarrow \mu^\pm \nu jj + \tau^\pm \nu jj$ (fb)	80	71	13	2.8×10^{-1}	2.1×10^{-1}	1.1×10^{-1}
$e_R^+ e_L^- \rightarrow e^\pm \nu jj$ (fb)	220	190	31	1.6	6.4×10^{-1}	3.4×10^{-1}
$e_L^+ e_R^- \rightarrow e^\pm \nu jj$ (fb)	40	36	6.4	1.4×10^{-1}	1.1×10^{-1}	5.7×10^{-2}
$e_R^+ e_R^- \rightarrow e_R^- \bar{\nu} jj$ (fb)	100	92	11	3.8	2.2×10^{-1}	1.2×10^{-1}
$e_L^+ e_L^- \rightarrow e_L^+ \nu jj$ (fb)	40	31	4.3	1.3	7.2×10^{-2}	4.1×10^{-2}
Total $\ell \nu jj$ background (fb)	820	720	120	7.4	1.5	8.0×10^{-1}
$e_R^+ e_L^- \rightarrow \mu^+ \mu^- jj + \tau^+ \tau^- jj$ (fb)	1.2	3.7×10^{-2}	5.5×10^{-3}	1.1×10^{-4}	9.4×10^{-5}	5.0×10^{-5}
$e_L^+ e_R^- \rightarrow \mu^+ \mu^- jj + \tau^+ \tau^- jj$ (fb)	19	1.0	1.4×10^{-1}	3.0×10^{-3}	2.5×10^{-3}	1.4×10^{-3}
$e_R^+ e_L^- \rightarrow e^+ e^- jj$ (fb)	8.4	9.0×10^{-2}	4.6×10^{-3}	5.8×10^{-4}	2.6×10^{-4}	1.3×10^{-4}
$e_L^+ e_R^- \rightarrow e^+ e^- jj$ (fb)	220	2.4	1.2×10^{-1}	1.5×10^{-2}	6.7×10^{-3}	3.4×10^{-3}
$e_R^+ e_R^- \rightarrow e^+ e^- jj$ (fb)	59	7.2×10^{-1}	2.4×10^{-2}	4.5×10^{-3}	2.0×10^{-3}	1.0×10^{-3}
$e_L^+ e_L^- \rightarrow e^+ e^- jj$ (fb)	19	1.0	8.0×10^{-3}	1.4×10^{-3}	6.7×10^{-4}	3.7×10^{-4}
Total $\ell \ell jj$ background (fb)	330	5.2	3.0×10^{-1}	2.5×10^{-2}	1.2×10^{-2}	6.4×10^{-3}
S/\sqrt{B} (assuming 1 ab^{-1})	1.4×10^{-1}	1.6×10^{-1}	2.6×10^{-1}	1.0	1.8	2.5
S/B (assuming 1 ab^{-1})	1.3×10^{-4}	1.9×10^{-4}	7.4×10^{-4}	1.2×10^{-2}	4.6×10^{-2}	8.7×10^{-2}

TABLE II: The results without ISR. The cross sections of both the signal and the backgrounds are shown for $\sqrt{s} = 300$ GeV. For the signal, m_{H^\pm} is 150 GeV and $|\xi|^2$ is taken to be 10^{-3} . For the $\ell \ell jj$ processes, the misidentity rate of one of the leptons is assumed to be 0.1. The signal significance S/\sqrt{B} and the ratio S/B are evaluated for the integrated luminosity to be 1 ab^{-1} .

	Basic	M_{jj}	p_T^{jj}	E_{jj}	$\cos \theta_{\text{lep}}$	$M_{\ell\nu}$
$e_R^+ e_L^- \rightarrow \ell^\pm \nu jj$ (fb)	6.8×10^{-3}	6.0×10^{-3}	3.3×10^{-3}	3.1×10^{-3}	2.4×10^{-3}	2.4×10^{-3}
$e_L^+ e_R^- \rightarrow \ell^\pm \nu jj$ (fb)	1.3×10^{-1}	1.2×10^{-1}	6.6×10^{-2}	6.3×10^{-2}	5.0×10^{-2}	4.9×10^{-2}
Total signal (fb)	1.4×10^{-1}	1.3×10^{-1}	6.9×10^{-2}	6.6×10^{-2}	5.2×10^{-2}	5.1×10^{-2}
$e_R^+ e_L^- \rightarrow \mu^\pm \nu jj + \tau^\pm \nu jj$ (fb)	350	310	55	2.9	2.2	1.1×10^{-1}
$e_L^+ e_R^- \rightarrow \mu^\pm \nu jj + \tau^\pm \nu jj$ (fb)	84	76	17	1.8	1.4	9.7×10^{-2}
$e_R^+ e_L^- \rightarrow e^\pm \nu jj$ (fb)	210	190	32	2.8	1.6	2.8×10^{-1}
$e_L^+ e_R^- \rightarrow e^\pm \nu jj$ (fb)	42	38	8.5	9.0×10^{-1}	7.0×10^{-1}	4.9×10^{-2}
$e_R^+ e_R^- \rightarrow e_R^- \bar{\nu} jj$ (fb)	92	81	10	3.2	2.2×10^{-1}	1.0×10^{-1}
$e_L^+ e_L^- \rightarrow e_L^+ \nu jj$ (fb)	32	29	3.7	1.1	7.8×10^{-2}	3.4×10^{-2}
Total $\ell \nu jj$ background (fb)	810	720	130	13	6.2	6.7×10^{-1}
$e_R^+ e_L^- \rightarrow \mu^+ \mu^- jj + \tau^+ \tau^- jj$ (fb)	1.2	4.2×10^{-2}	5.9×10^{-3}	3.7×10^{-4}	3.1×10^{-4}	4.6×10^{-5}
$e_L^+ e_R^- \rightarrow \mu^+ \mu^- jj + \tau^+ \tau^- jj$ (fb)	22	1.2	1.5×10^{-1}	9.9×10^{-3}	8.3×10^{-3}	1.2×10^{-3}
$e_R^+ e_L^- \rightarrow e^+ e^- jj$ (fb)	9.6	9.2×10^{-2}	4.1×10^{-3}	6.3×10^{-4}	3.2×10^{-4}	1.0×10^{-4}
$e_L^+ e_R^- \rightarrow e^+ e^- jj$ (fb)	230	2.4	1.0×10^{-1}	1.7×10^{-2}	9.2×10^{-3}	2.9×10^{-3}
$e_R^+ e_R^- \rightarrow e^+ e^- jj$ (fb)	70	6.4×10^{-1}	2.3×10^{-2}	4.2×10^{-3}	2.1×10^{-3}	9.1×10^{-4}
$e_L^+ e_L^- \rightarrow e^+ e^- jj$ (fb)	24	2.2×10^{-1}	7.4×10^{-3}	1.4×10^{-3}	6.3×10^{-4}	3.1×10^{-4}
Total $\ell \ell jj$ background (fb)	360	4.6	2.9×10^{-1}	3.4×10^{-2}	2.1×10^{-2}	5.5×10^{-3}
S/\sqrt{B} (assuming 1 ab^{-1})	1.3×10^{-1}	1.5×10^{-1}	1.9×10^{-1}	5.8×10^{-1}	6.6×10^{-1}	2.0
S/B (assuming 1 ab^{-1})	1.2×10^{-4}	1.8×10^{-4}	5.3×10^{-4}	5.1×10^{-3}	8.4×10^{-3}	7.5×10^{-2}

TABLE III: The results with the ISR. The cross sections of both the signal and the backgrounds are shown for $\sqrt{s} = 300 \text{ GeV}$. For the signal, m_{H^\pm} is 150 GeV and $|\xi|^2$ is taken to be 10^{-3} . For the $\ell \ell jj$ processes, the misidentity rate of one of the leptons is assumed to be 0.1. The signal significance S/\sqrt{B} and the ratio S/B are evaluated for the integrated luminosity to be 1 ab^{-1} .